International Journal of Extreme Manufacturing

TOPICAL REVIEW • OPEN ACCESS

A review on the erosion mechanisms in abrasive waterjet micromachining of brittle materials

OPEN ACCESS
IOP Publishing | IMMT
International Journal of Extreme Manufacturing
Int. J. Extrem. Manuf. 1 (2019) 012006 (14pp)
https://doi.org/10.1088/2631-7990/ab1028

Topical Review

A review on the erosion mechanisms in abrasive waterjet micromachining of brittle materials

T Nguyen and J Wang

School of Mechanical and Manufacturing Engineering, UNSW Sydney, NSW 2052, Australia

E-mail: jun.wang@unsw.edu.au

Received 15 March 2019
Accepted for publication 15 March 2019
Published 15 April 2019

Abstract

The fabrication of miniature structures on components with high-integrity surface quality represents one of the cutting edge technologies in the 21st century. The materials used to construct such small structures are often difficult-to-machine. Many other readily available technologies either cannot realise necessary precision or are costly. Abrasive waterjet (AWJ) is a favourable technology for the machining of difficult-to-machine materials. However, this technology is generally aimed at large stock removal. A reduction in the scale of this technology is an attractive avenue for meeting the pressing need of industry in the production of damage-free micro features. This paper reviews some of the work that has been undertaken at UNSW Sydney about the development of such an AWJ technology, focusing on the system design currently employed to generate a micro abrasive jet, the erosion mechanisms associated with processing some typical brittle materials of both single- and two-phased. Processing models based on the findings are also presented. The review concludes on the viability of the technology and the prevailing trend in its development.

Keywords: micro abrasive jet, abrasive waterjet, ductile erosion, viscous flow, difficult to machine materials

(Some figures may appear in colour only in the online journal)

Nomenclature

C_p	percentage of particle concentration by mass
C_c	percentage of chemical additive concentration by mass
d, d_j	jet diameter (m)
d_n	nozzle diameter (m)
d_p	mean diameter of abrasive particle (m)
E_m	elastic modulus of target material (Pa)
H_m	hardness of target material (Pa)
h	channel depth (m)
K	consistency index ($\mathrm{Nm^{-2}\,s^{n}}$)
K_m	fracture toughness of target material ($\mathrm{Pam^{0.5}}$)
k_d	discharge factor
L	jet compact (or stabilised) length (m)
L/d	characteristic length ratio
MRR	material removal rate ($\mathrm{m^3\,s^{-1}}$)

2631-8644/19/012006+14$33.00

$\dot{m}_p$	mass flow rate of particle (kg s^{-1})
n	flow behaviour index
P	pressure (Pa)
Re	Reynolds number
S_n	nozzle standoff distance (m)
V	removal volume of target material (m^3)
v, v_j	jet velocity (ms^{-1})
v_n	nozzle traverse speed (ms^{-1})
v_p	particle velocity (ms^{-1})
w	channel width (m)
We	Weber number

Greek letters

ϕ	channel wall angle (rad)
μ	dynamic viscosity of slurry (Pa.s)
σ	dynamic surface tension of slurry (Nm^{-1})
ρ_s	density of slurry (kg m^{-3})
ρ_p	density of particle (kg m^{-3})
$\dot{\gamma}$	shear rate (s^{-1})

1. Introduction

Miniature component structures are the fundamental elements used in modern micro electro-mechanical (MEM), optical, and biomedical systems. A technology that is capable of fabricating these micro-structures with high precision and low cost is in a high demand in industry, but places a technological challenge worldwide. This challenge is intensified by the increasing requirements for high surface integrity on the manufactured components, as well as the need to process advanced materials that are continually developed and are often difficult-to-machine.

Conventional machining technologies are either not capable of processing some of the materials or inevitably cause damages to the machined components in addition to the productivity and cost concerns. To process a difficult-to-machine material, it requires a tool having high hardness and good wear-resistance so that the tool can engage into the material and its sharpness can be retained long during the process. In current machining practice, cutting tools with the hardness of as high as five times that of the workpiece are often referred to [1], and the diamond appears to be a vital choice for many such applications. However, sharpening of such tools is difficult [2]. On top of that, high material hardness is often associated with high brittleness, so that controlling the process parameters to avoid crack formation is difficult and often requires using very small cutting parameters. For instance, experiments using a single point cutting tool to process a brittle silicon carbide material showed that to facilitate the ductile machining mode, the depth of cut must be set shallower than 100 *nm* [3]. Other non-mechanical techniques include LIGA (lithography, electroplating, and moulding) and chemical erosion/etching. LIGA is normally expensive to perform and cannot process materials which cannot be pressed into the LIGA mould. The chemical erosion/etching process cannot be used on chemical resistant materials without the assist of some toxic chemical gases in addition to the difficulty in controlling the surface textures and its low processing rate [4]. Other techniques include the use of high intensity energy sources such as electrical discharge machining (EDM) [5] or a laser beam ablation [6] which use thermal energy to locally soften and remove the unwanted material. The high intensity heat used in these processes is a main cause for craters, micro-cracks, thermal damages and detrimentally tensile residual stresses [7] on the machined component surfaces, so that a post process is often required by, say, using an abrasive polishing technique. For femtosecond laser machining, other than the cost of operation and equipment, the ablation in this technique is material-specific which depends not only on the thermal but also the optical properties of target material. Minimising the heat affect zone in this type of machining requires a proper selection of laser parameters in response to the optical breakdown and laser ablation thresholds of the target material and is at the cost of production rate. In addition, ablated materials may be redeposited at or near the site of breakdown, creating unintended structures or debris at the machining site [8].

By contrast, AWJ has been increasingly used for the machining of difficult-to-machine materials [9]. In this technique, a jet of water and abrasive particle slurry at a high pressure is introduced onto the workpiece. While material removal is essentially undertaken by the abrasive particles, the continuous flow of water carries away the heat generated during the process and eliminates the thermal effect, making it the ideal process for thermal sensitive materials. However, the application has been based mainly on the use of ultrahigh pressure jet of millimetres in diameter using large abrasives of above 100 μm for quick stock removal, whereas the surface quality is of minor concern. Almost all materials, including the hardest and extremely brittle diamond can be deformed plastically to some extent. However, this can only be achievable at a nano length scale during the contact loading [1]. Given the scale and expense of modern manufacturing in the production of damage-free micro features, a reduction in scale of the macro AWJ technology, such as using smaller nozzles, finer particles or lower pressures, to promote ductile-mode-like material removal has become attractive for industry.

This paper reviews the developments of the micro AWF technology for the machining of hard and brittle materials. The review is based on the work that has been undertaken in the authors' laboratory and focuses on the system employed to generate a micro AWJ and the erosion mechanisms associated with processing different types of brittle materials. Mathematical models to represent the process and estimate the relevant process quantities are also presented. The review concludes on the viability of the technology and the prevailing trend in its development.

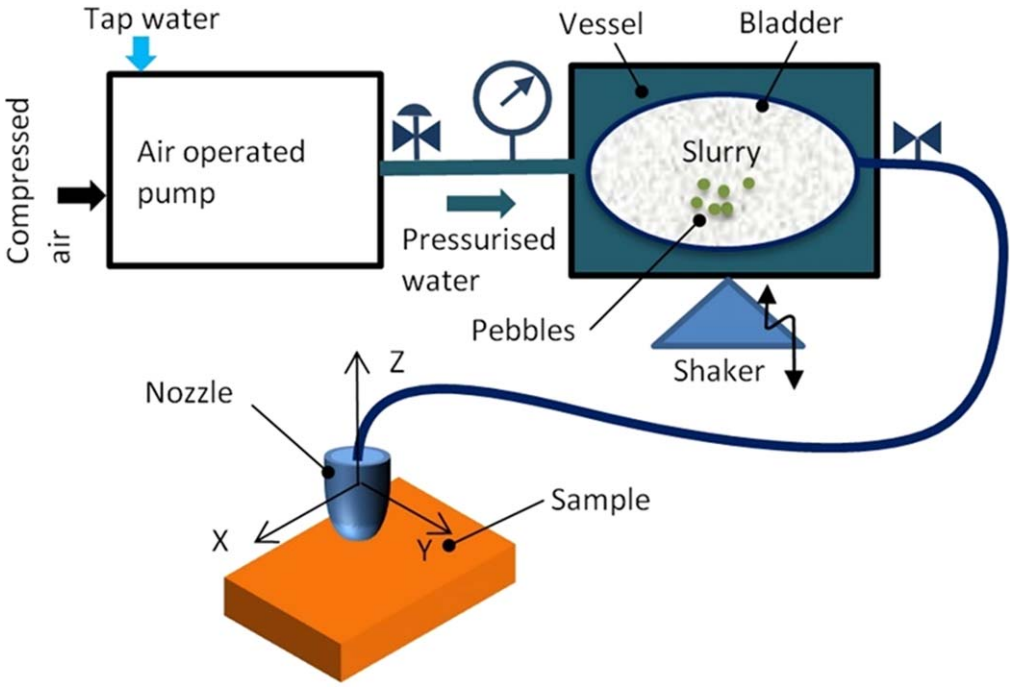

Figure 1. A bladder type micro AWJ machining system. Reprinted from [11], Copyright (2018), with permission from Elsevier.

2. Micro abrasive jet machining systems

In an ultrahigh pressured AWJ system, the AWJ is formed by supplying abrasives separately into a high pressured waterjet stream. The waterjet stream is formed by a small orifice and flows into a mixing chamber where vacuum is generated, drawing the solid abrasives in, so that it is referred to as an entrainment system. The mixture is forced through a nozzle (or called mixing tube), the diameter of which is typical about 0.8 mm to 1.6 mm [10]. A scale-down of this working principle to a micro-sized jet presents a difficulty since the pressure in a microjet system may not be high enough to create the required vacuum and to entrain the particles in, in addition to the requirement for precision alignment of the orifice and nozzle.

Micro AWJ systems often use a slurry jet principle where the particles are mixed with the liquid well before the slurry goes into the nozzle. The pressure must be high enough to overcome the friction as the slurry flows through a tiny nozzle of typically about a hundred micrometres in diameter. The pressurised slurry jet must also provide sufficient energy to initiate a material removal process on the target material. On the other hand, the pressure may not be set too high in order to avoid damages to the material, particularly those of brittle nature. Furthermore, the divergence of the jet as it is ejected from a micro nozzle must be controlled to meet the precision of micromachining.

There have been some studies aiming to scale down the ultrahigh pressure AWJ systems, including the reduction in size of the nozzle and water pressure [12] or using pressurised water tank [13]. Pressures used in these scaled-down systems are typically around 100 MPa, while those in the pressurised water tank are about 5 MPa which is not sufficient to process high wear resistant material. A number of micro AWJ systems have been constructed and studied in the authors' laboratory. Figure 1 illustrates one that works better than others. An air-driven liquid pump is used to pressurise water to a desired pressure between 2 and 67 MPa. The water is then passed into a stainless steel vessel. Placed inside the vessel is a rubber (or soft skin) bladder which is used to store and isolate premixed slurry from the pressurised water. Pressurised water squeezes the slurry through a nozzle assembly. The flow rate of slurry can be controlled by adjusting the air pressure entering the pump and/or a water pressure control valve. Prior to a machining process, the pressure vessel is vibrated at about 1 Hz by a shaker to allow the slurry to mix uniformly. Some pebbles are added inside the bladder to help with the mixing process. In a production environment, two or more vessels may be used so that when one is used, the other is refilled so that continuous operation is possible. A nozzle tube made of high wear resistant ZrO_2 ceramic is placed inside the nozzle assembly. To effectively isolate the jet flow disturbance at the nozzle inlet, the aspect ratio (length/diameter) of the tube should be made greater than 50 [14]. This is to ensure that the diameter of the impact zone can be maintained approximately as the same as the nozzle diameter.

3. Erosion Mechanisms

3.1. Erosion of single-phased material

Unlike the ultrahigh pressure (typically above 100 MPa) abrasive jet applications where the material can be eroded quickly [15, 16], in microjet machining with a lower jet pressure (typically from 1 to 30 MPa), the jet energy is not

sufficient to form a cut immediately. The jet dynamic behaviour and the response of material to the jet impact are vastly different from those in ultrahigh pressure jet applications. This review is based on the investigations into the micro-hole formation process carried out in the authors' laboratory [17, 18].

The test samples were 5 mm thick amorphous soda-lime sheets whose properties were 2.5×10^3 kg m^{-3} in density, 75 MPa.m$^{0.5}$ in fracture toughness, 74 GPa in Young modulus and 5.5 GPa in hardness. The slurry jet was set at $P = 3$ MPa and contained alumina abrasives of 10 μm in average diameter (d_p) at the concentration by mass $C_p = 2.5\%$. The abrasives were alumina with the hardness of 10.79 GPa and density of 3.65 g cm^{-3}. The nozzle tube was 0.2 mm in inner diameter and 10 mm in length, and positioned normally to the sample surface with the standoff distance $S_n = 1.5$ mm. To inspect the effect of jet viscosity, a polymeric additive (non-ionic polyacrylamide flocculant type, Ciba Magnafloc 333 manufactured by Ciba Speciality Chemicals) was mixed with the slurry at the concentration by mass $C_c = 0.25\%$.

Figure 2 shows the feature of a typical hole processed by a low-pressure slurry jet. Characterised by a cross sectional shape of 'W', the hole has its open diameter about four times the jet diameter.

Figure 3 illustrates the fluid flow developed upon a jet impact. The jet velocity direction is diverted from a potential flow, which is aligned with the nozzle axis, to a viscous flow which is parallel to the target surface [20]. It follows that the kerf profiles created by these jet flow characteristics can be distinguished by three zones: AB, BC and CD, as shown in figure 2(a). The jet impact zone AB is within the central region of the hole under the direct impact of the jet [21], and is smaller than the jet diameter. In this zone, the normal impact direction does not facilitate material removal in the cutting wear (or ductile) mode and the associated removal rate is small, so that a ridge is formed in the hole central region. The zone BC is created by the viscous flow sweeping along the target surface. The target surface becomes steeper with the increase of depth in this zone. While promoting the cutting wear mode erosion, this also allows the erosion rate to be raised. The surface disturbances of the liquid within the viscous flow zone develop a wave travelling radially outward, as shown in figures 2(b) and 3(b) [22]. Beyond the BC zone is the CD zone where the wave is diminished and particles are accumulated. A turbulent flow is formed in this zone which is bounded by the hole edge.

Upon the impact of an abrasive particle, there are two force components acting on the target surface. While the force component normal to the target surface facilitates an indentation in the workpiece, the component tangential to the surface promotes shearing stresses which may create microchips from the workpiece or cause a ploughing action to the surface. Depending on the attribution of the two forces and the response of target material to these forces, the removal of material takes place in brittle or ductile mode [23]. In the brittle mode removal, cracks are initiated and propagated on the machining surface. By contrast, when the material undergoing a ductile removal mode, deformation associated

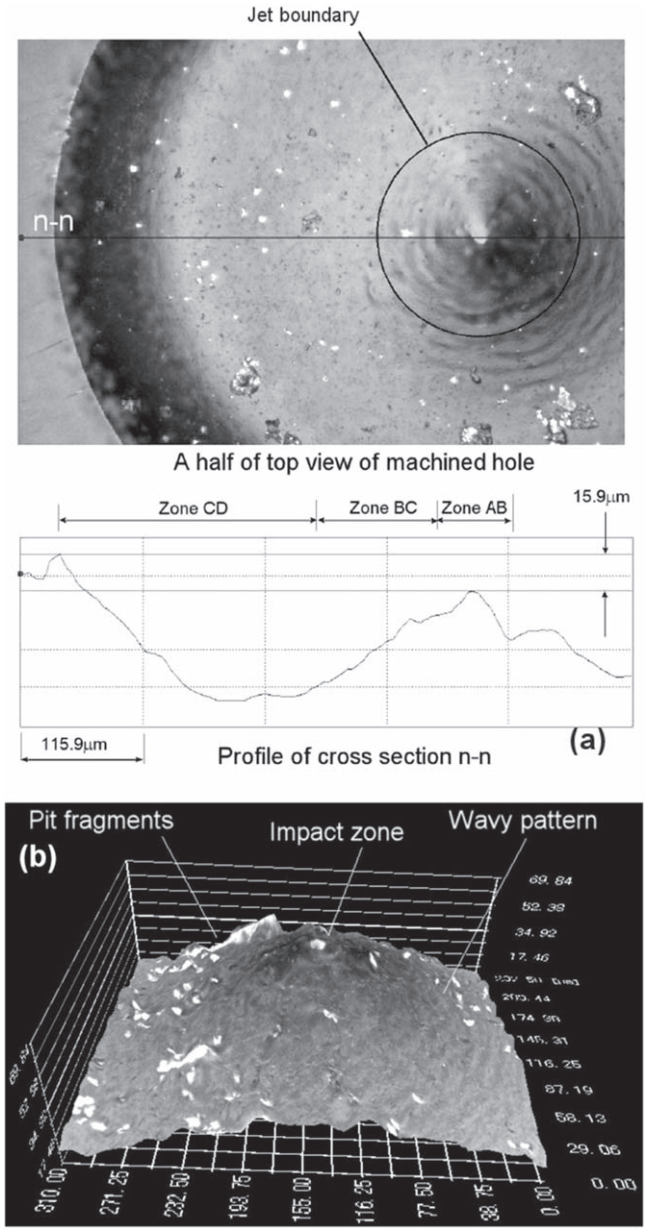

Figure 2. Features of the hole after processing for 180 s by a 3 MPa slurry jet of 0.2 mm in diameter, containing 10 μm particles with the concentration $C_p = 2.5\%$: (a) top view and cross section and (b) surface morphology of the impact zone (dimensional unit in μm). Reproduced with permission from [17].

with shearing or cutting takes place. A new impact erosion mechanism for ductile materials has been developed to fundamentally explain the material removal process, that is through material failures induced by inertia, elongation and adiabatic shear banding [24]. For consistency, the term cutting wear is still used in this paper. Further, the cracked fragments may contribute to the erosion process. It has been reported that materials eroded by the cracked fragments form surfaces with the accumulation of the crack edges [25, 26]. Because of the jet divergence, a momentum is created that results in normal and shear stresses to the target surface [27]. As discussed above, the attribution of the two stresses on the target material depends on the fluid flow zone developed on

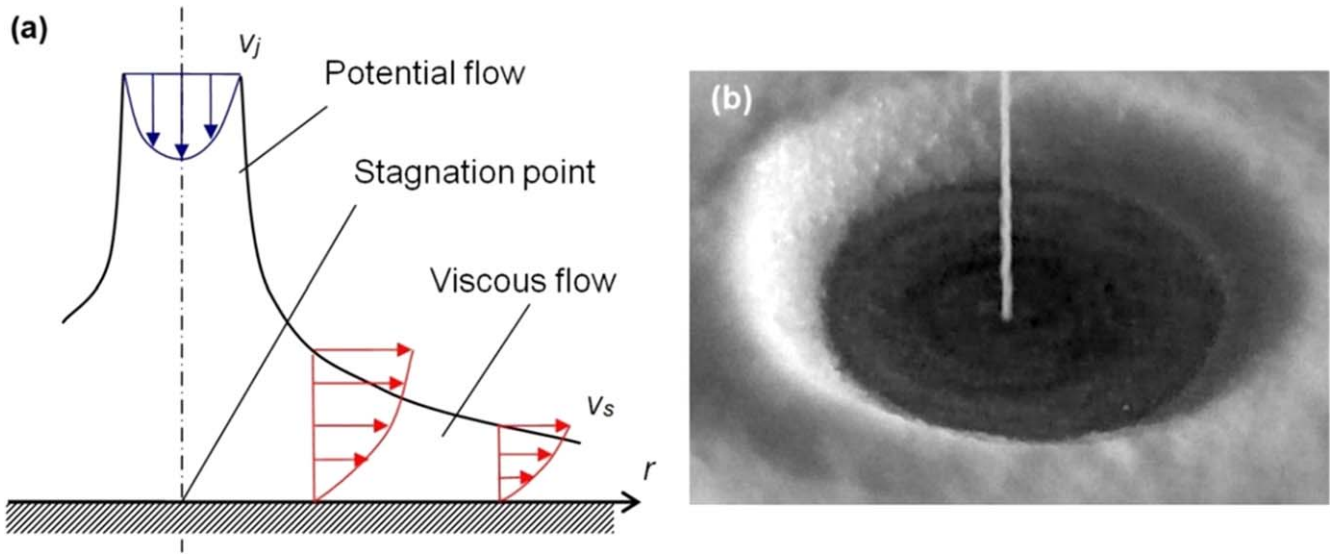

Figure 3. Fluid flow developed upon a jet impact: (a) schematic [17] and (b) visualisation of the wave development by the jet impact (machining condition as in figure 2) [19]. (a) Reproduced with permission from [17]. (b) Reproduced with permission from [19].

material surface. This in turn results in a variation of the appearance of the processed surface. On the surface morphology shown in figure 2, some pits are clearly found within the AB zone. Within the CD zone, the accumulation of particles and possibly pit fragments promotes a turbulent motion that generates further strikes of particles onto the surface at random directions. This particle laden flow leads to a decrease in erosion in the ductile mode, as compared with the wavy BC zone which appears smoother than both the AB and CD zones. The viscous flow in the BC zone provides a hydrodynamic film layer that may act as a lubricant or damping layer to reduce the friction between abrasive particles and material surface, thereby widening the range of attack angles for the cutting wear mode to occur [28]. Further, the fluid flow direction in this zone is favoured for cutting wear by particles. As a result, a smooth surface without cracks was generated in the BC zone irrespective of the brittleness of material. These surface characteristics indicate the predominance of the shearing action, thus ductile erosion mode in the material removal process. The appearance of the wavy surface is a result of the wave energy transferred to the surface by the wavy viscous flow. An experiment was conducted where a polymeric additive was mixed with the slurry to increase its viscosity. The result shown in figure 4 confirms the existence of a wavy viscous flow.

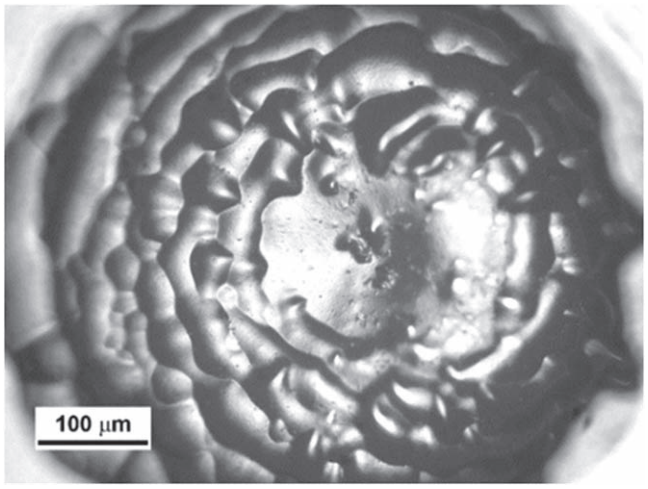

Figure 4. Wavy pattern developed on a glass surface processed after 60 s by a 2 MPa slurry jet of 0.2 mm in diameter, containing 10 μm particles at $C_p = 2.5\%$ concentration by mass and polymeric additive at the concentration $C_c = 0.25\%$ by mass. Reproduced from [18], with the permission of AIP Publishing.

3.2. Erosion in two-phased material

Reaction-bonded silicon carbide (RB-SiC) is a composite made of two major constituents, i.e. silicon carbide (SiC) grains surrounded by a matrix of silicon (Si) [29]. Owing to its excellent properties of light weight, thermal stability and chemical inertness, RB-SiC is a favourable material for constructing devices working in harsh environment, e.g. optical mirrors used in the space [30]. However, as many other advanced materials, RB-SiC is a difficult-to-machine material. Not only because of the hardness and brittleness of the SiC constituent, but the difficulty is also due to the non-uniformity of the RB-SiC structure that consists of the hard phase SiC and the softer Si matrix. Under the same applied stress, the response of these two constituents is distinctively different. The work in [11] presents an investigation on the material removal mechanisms of RB-SiC and the resulting surface quality when subjected to the impact of a micro slurry jet.

The material used in this study had the SiC grains of approximate 35 μm in size surrounded by a matrix of Si with the volume fraction, C_{Si} about 21.5%. Surface roughness of the samples, R_a, was about 14 μm. The slurry jet contained 25 μm alumina particles with the mass concentration of 15% and was operated at the water pressure of 25 MPa. For comparison, another mode of fixed particle polishing was

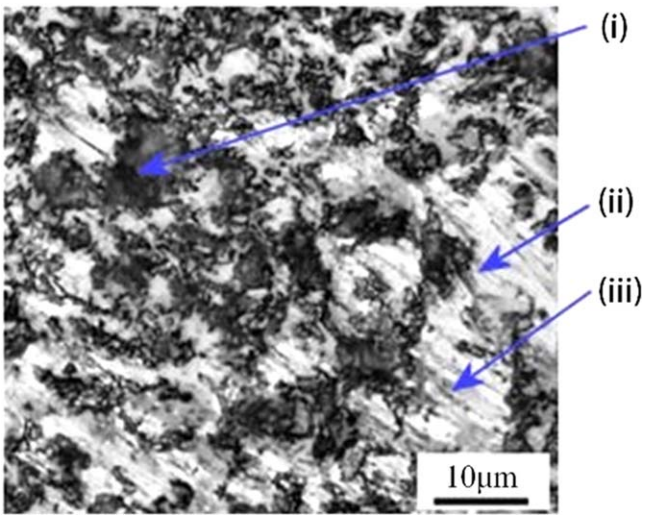

Figure 5. Surface polished after 3 min by diamond abrasives: (i) brittle fracture of a SiC grain, (ii) embedment of plastically deformed Si, and (iii) grooves. Reprinted from [11], Copyright (2018), with permission from Elsevier.

conducted, and it was made by using a Struers–TegraForce-1 polishing machine. The loading force of 20 N was applied on the sample surface which was placed against a 65 μm diamond grained disk of 200 mm in diameter rotating at 30 rpm.

Figure 5 shows a surface processed by diamond polishing. Large-scaled fractures in the form of irregular pits appear on the surface of SiC grains. In contrast, the Si portion is found to have been deformed plastically. On the surface of Si phase, there are a number of deep and parallel grooves aligned with the abrasive motion. The deformed Si chips were found embedding over the surface of the fractured SiC grains.

Figure 6 illustrates the wear process by diamond polishing. Because of their extremely high brittleness [31], SiC grains when subjected to the indentation of diamond abrasives experience an initiation of cracks. Following their relative motion to the diamond abrasives, the cracks are propagated along the SiC grain cleavages. As the process continues, the cracks become deepen and, a certain degree, large fragments are formed and consequently removed from the grains, leaving the surface with large pits. However, the process is different from the grinding of single-phased SiC material where brittle material removal mode is dominant [32]. Of the RB-SiC composite structure is the Si matrix which can be plastically deformed, unlike the brittle SiC grains. Some previous studies show that amorphous transformation in Si can be initiated by stress, even at extremely low temperature of liquid nitrogen boiling point (−195 °C) [33], and the initiation occurs when indenting the material at a hydrostatic pressure greater than 11–13 GPa [34, 35]. Owing to the wear resistance higher than that of SiC, the sharpness of the diamond abrasives was retained during the process to allow the abrasives to engage with the sample material with small contact areas. As a result, sufficient stresses were developed, raising a plastic deformation on the Si phase. It is noted that the diamond abrasives were relatively larger than the SiC grains (65 μm versus 35 μm SiC). During the process, the removed amorphous Si was accumulated and compressed into the nearby pockets. The pockets include the spaces between the diamond abrasives and the processed sample surface, as well as the available pits formed by the fractured SiC grains.

When comparing with the surface of RB-SiC processed by a slurry jet, shown in figure 7, it is noted that not only was the jet pressure used (25 MPa) much lower than the hydrostatic pressure required for initiating the amorphous transformation on the Si matrix (11–13 GPa), the abrasives of alumina was also softer than the SiC grain constituent (20.45 GPa versus 24.53 GPa). Notwithstanding these facts, a hole with a depth of about 141 μm, about four times of the average SiC grain size ($\approx$ 35 μm) were formed. The processed surface appeared with irregular patterns of exposed SiC grains which are surrounded by micro channels formed on the Si matrix. Although both the material constituents are brittle, there was no micro crack found on the eroded surfaces.

The mechanism of wear on RB-SiC by the impact of a slurry jet is clearly different from that by diamond polishing and that on the single-phase material described earlier. In polishing, the same load is applied to both of the material constituents for the same depth of cut. In slurry jet impact-induced material removal, wear takes place mainly by the motion of the abrasives which can roll, rebound, collide and/or slide freely. Certainly, the alumina abrasives, particularly when driven by a low pressurised jet, cannot indent into the harder SiC grains. The abrasive-material engagement can be made only on the Si matrix whose hardness is lower than that of the abrasives. Following the engagement, the removal of material is made by two actions of shearing and wedging. The shearing takes place by the rolling action of the engaged abrasives, which eventually creates a number of channels along the Si matrix and around the harder SiC grains, as illustrated in figure 7(a). It is noted on the depth of the hole processed in this work is four times the SiC grain size. Since wear cannot be made directly on the SiC grains, it is implied that the removal of the SiC grains takes place by weakening their bonding with the material structure to cause an eventual removal of the whole grains from the substrate. Because of the small volume fraction of Si ($C_{Si} \approx 21.5\%$), the space between the hard SiC grains is generally narrower than the abrasive size. Such narrow spaces prevent the abrasives from penetrating deeper into the roots of the SiC grains. The wear caused by the shearing on Si may be diminished. As the process continues, the coming abrasives act as wedges that weaken the bond and finally lift up the whole SiC grains from the substrate, as shown in figure 8. By this wedging action, micro-cracks may be formed at the interface between the remained SiC grains and the surrounding Si bond. Nevertheless, the shear induced by the rolling action of abrasives again takes place to smoothen the newly cracked surfaces, resulting in the crack-free surface as shown in figures 7 and 8(b).

It is feasible to use a low-pressure slurry jet containing abrasives that are softer than the SiC grains, to machine RB-SiC composite without causing any brittle fracture. The abrasive wear on RB-SiC involves different mechanisms in the Si and

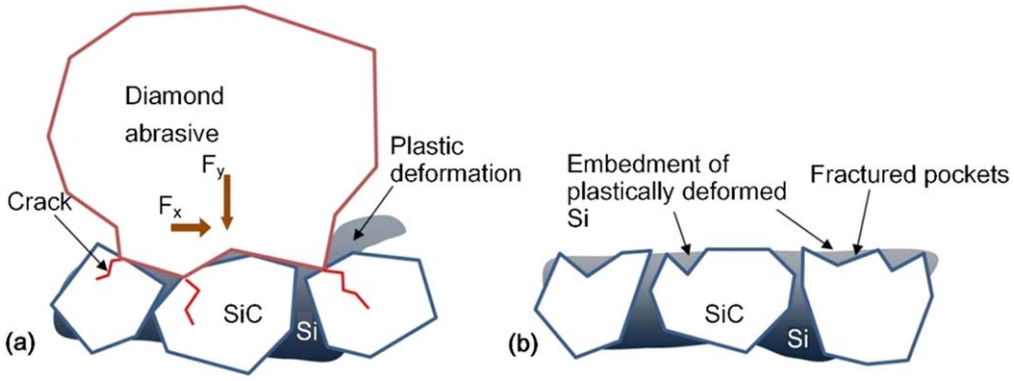

Figure 6. Schematic of wear process on RB-SiC by diamond abrasives: (a) forming of cracks on SiC grains and plastic deformation on Si matrix; and (b) embedment of Si in the fractured pockets of SiC grains. Reprinted from [11], Copyright (2018), with permission from Elsevier.

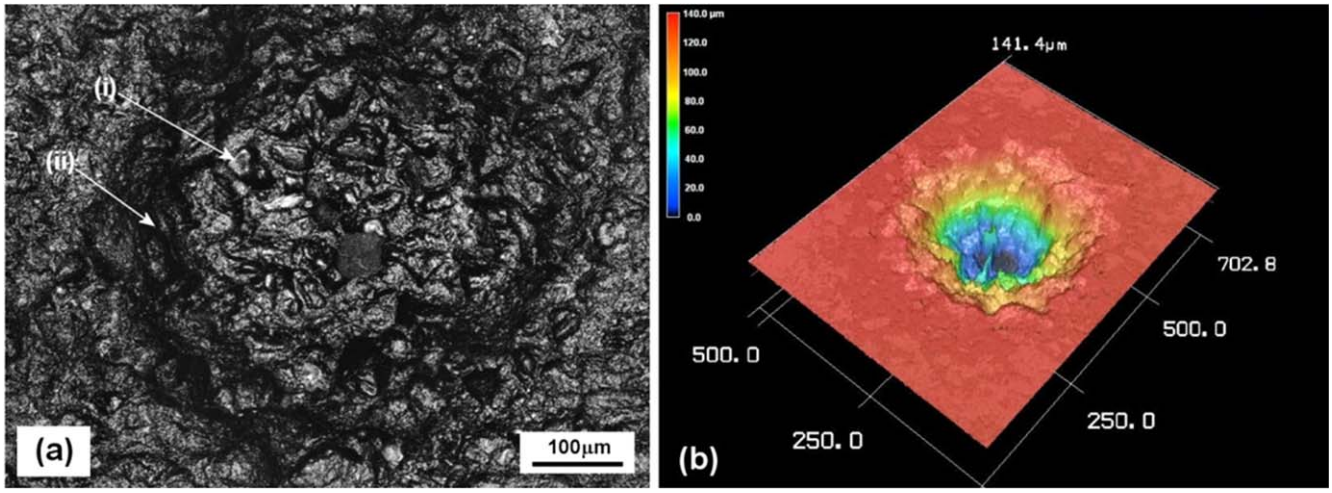

Figure 7. Topology (a) and 3D profile (b) of RB-SiC surfaces processed after 10 s by slurry jet ((i) exposed SiC grains and (ii) channels). Reprinted from [11], Copyright (2018), with permission from Elsevier.

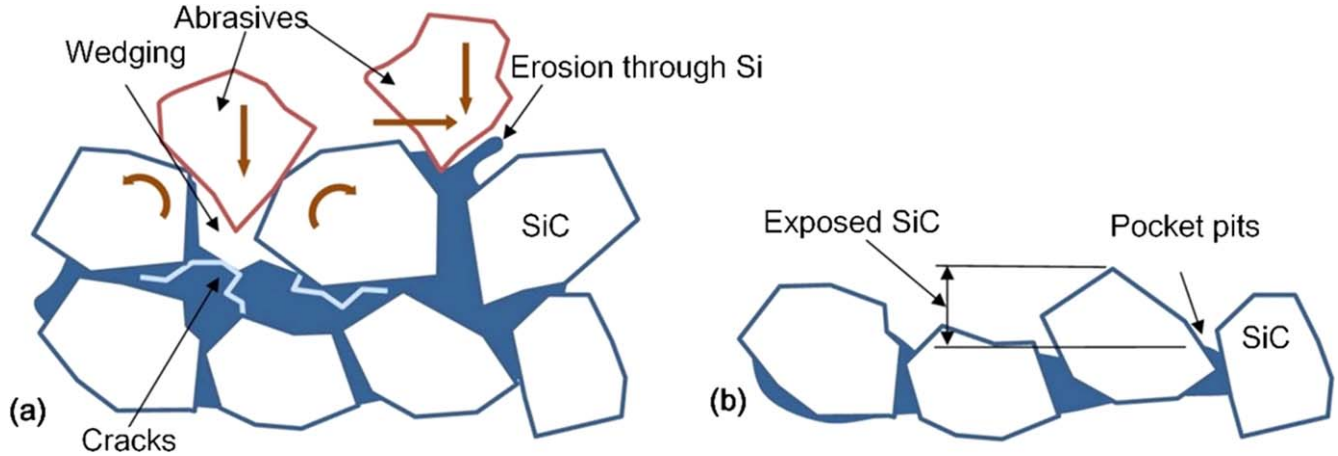

Figure 8. Schematic of the wear process of RB-SiC by the impact of an alumina slurry jet: (a) material removal, and (b) exposed surface. Reprinted from [11], Copyright (2018), with permission from Elsevier.

SiC constituents. In diamond disk polishing, brittle fracture is dominant on the SiC phase and there are depositions of the plastically deformed Si phase on the fractured SiC surface. By contrast, wear caused by slurry jet takes place mainly through weakening the Si bond by erosion and wedging action, which eventually releases the SiC grain from the material structure.

4. Process models

4.1. Jet stability

A liquid jet as ejected from a nozzle is no longer constrained by the nozzle inner wall, but contacts with the atmospheric air. The

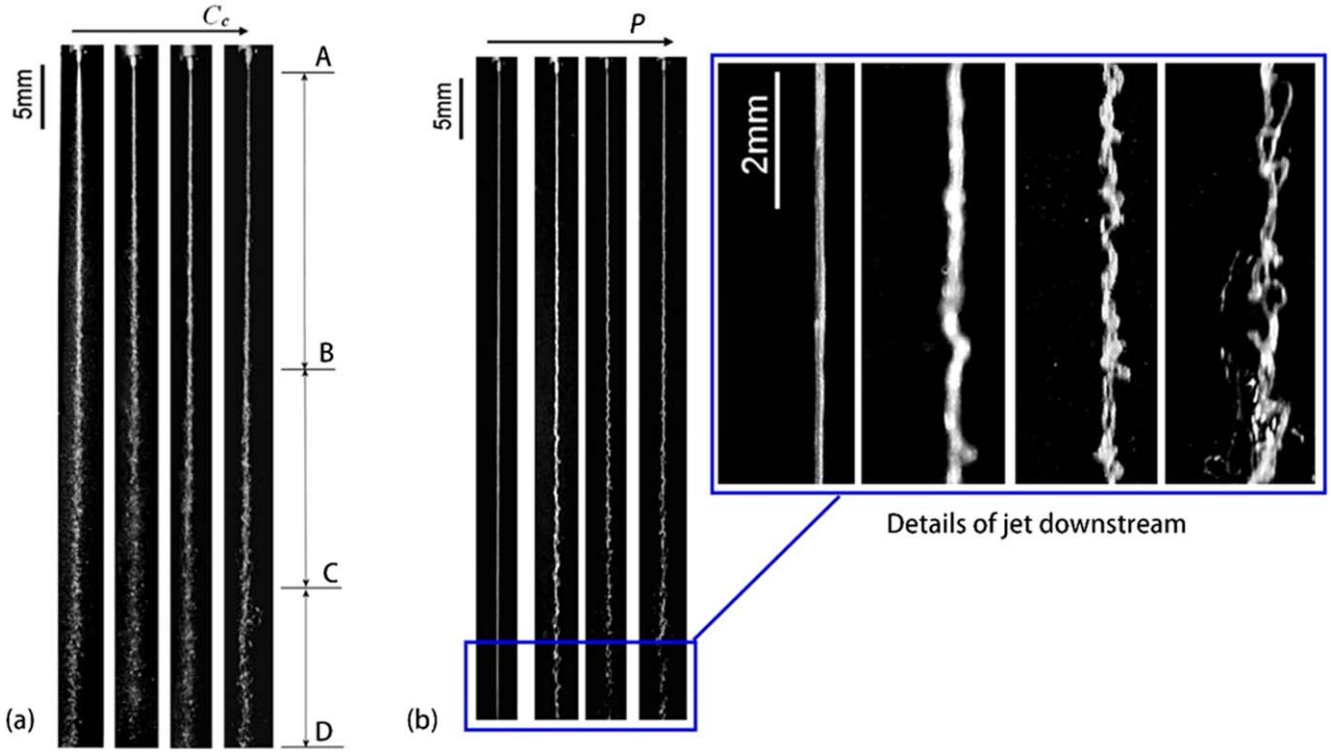

Figure 9. Jet stability by the effect of: (a) chemical concentration, C_c, varying from 0, 0.1%, 0.25% to 0.5% ($P = 2$ MPa, $d = 0.84$ mm); and (b) pressure, P, varying from 1, 2, 3 to 4 MPa ($d = 0.84$ mm, $C_c = 0.25\%$, $C_p = 5\%$ and $d_p = 10$ μm). Reprinted from [36], Copyright (2008), with permission from Elsevier.

Table 1. Testing conditions in the study of jet stability. Reprinted from [36], Copyright (2008), with permission from Elsevier.

Nozzle diameter, d (mm)	0.19, 0.50 and 0.84
Pressure, P (MPa)	1, 2, 3 and 4
Polymer additive (% by mass), C_c	0 (water only), 0.1, 0.25 and 0.5
Particle content (% by mass), C_p	1 and 5
Particle mesh (and size in brackets)	600 ($d_p = 25$ μm), 1000 (15 μm), and 1500 (10 μm)

jet becomes diverged and depending on the distance from the nozzle exit, different flow regimes are developed. Unlike the use of solid cutting tools, where the depth of cut can be easily controlled and the tool/workpiece contact area can be determined, in the jet cutting these parameters depend on the kinetic behaviour of the ejected jet. Whereas the divergence enlarges the impact zone, the change in the flow regime leads to a variation of velocity distribution within the jet cross sectional area when impacting on a target. These changes potentially make the control of liquid jet difficult. This is particularly important in microjet machining where precision is of major concern. In addition, as discussed above, viscosity of the slurry used in a non-through cut in microjet machining plays an important role in the behaviour of the viscous flow that governs the morphology of the machined surface. In this work [36], a jet compact length model was established to present a mathematical relationship between the jet stability measures and the jetting parameters.

Table 1 [36] shows the test conditions. To examine the effect of surface tension and viscosity of the jet, a polymeric additive (nonionic polyacrylamide flocculant type, Ciba Magnafloc 333 manufactured by Ciba Speciality Chemicals) was mixed with the slurry. The jet images were obtained at steady state of flow using the stroboscope method [37] with the illumination flashing of 3 μs.

Figure 9(a) shows instantaneous images of the jets subjected to different conditions of chemical concentration. Typically, a jet consists of three zones: AB, BC and CD. These zones are indicated in figure 9(a) for the most right flow where $C_c = 0.5\%$. In the compact zone AB, the jet is in good coherence and its length is measured as a compact length, L. The stability of the jet maintains until reaching the stage where disintegration occurs in the zone BC. Farther from the jet nozzle is the zone CD where the jet has totally lost its stability, forming drops. In contrast with the use of water only slurry solution ($C_c = 0$) where the disintegration of waterjet occurred somewhere close to the nozzle exit, the compact lengths (L) were increased by increasing the polymer additive in the jet. On the surface of a liquid jet, oscillations and perturbations occurs as a result of the competition between cohesive and disruptive forces [38]. The cohesion is formed by surface tension that restrains the liquid from breaking up into drops. In contrast, the disruption is promoted

by aerodynamic forces acting on the liquid surface. When the magnitude of the disruptive forces exceeds the surface tension, break-ups occur. The role of liquid viscosity, on the other hand, is to inhibit the growth of instabilities and generally delay the onset of disintegration [37, 39–41]. For the polymeric fluids used in this study, the enhancement of jet stability is mainly attributed to the increase of viscosity since the surface tension is reduced when increasing the chemical concentration [42].

The effects of jet pressure on the jet stability are shown in figure 9(b). At a low pressure of 1 MPa, the jet has a very large compact length. This is probably because the jet behaved under Rayleigh manner of laminar flow where the disintegration of jet was caused mainly by dilatational waves. This type of waves is developed by rotationally symmetrical oscillation of the jet where any disturbances is damped out by the fluid viscosity. The jet becomes unstable and disintegrates only when the incidental internal perturbations cause narrow bands to develop in the jet to a certain critical stage of the wave length [43]. According to the Weber theory [38], the wave formation is induced by the relative velocity of air to the outer layer of jet on which the air friction shortens the critical wave length. Jets injected at low pressures have low velocities, thus receiving a low air friction so that it is more stable. The promotions of the air friction to the jet surface at higher jet velocities increase the wave amplitudes and shorten the wave lengths. Enlarged views of this phenomenon are shown on the right hand side of figure 9(b) for the jet wave patterns at 20 mm downstream from the nozzle exit. It can be noticed that wave amplitudes increase and wave lengths decrease as the jet pressure increases from 1 to 4 MPa, where the wave patterns may be considered as a dilatational wave in 1 MPa, sinuous wave in 2 MPa and a distortion of wave axes in 3 and 4 MPa.

The aforementioned physical understanding shows that the stability of a jet is governed by the internal and external factors. By superimposing the two causes, the stability which is represented by the compact length, L can be analysed and determined. The internal disturbances are associated with the fluid properties including slurry density (ρ_f), surface tension (σ), viscosity (μ), particle size (d_p) and particle concentration (C_p). The external disruption is formed by the friction between the jet surface and the atmospheric air, that in turn is a direct result of the jet velocity (v_j) or jet pressure (P). Using the Buckingham Π theorem, the above parameters can be grouped as [31]

$$f(\Pi_1, \Pi_2, \Pi_3, \Pi_4, \Pi_5) = 0, \quad (1)$$

where the dimensionless parameters are defined as

$\Pi_1 = \frac{L}{d}$	characteristic length ratio, representing the jet stability
$\Pi_2 = Re = \frac{\rho v d}{\mu}$	Reynolds number, expressing the liquid inertial force/viscous force ratio
$\Pi_3 = We = \frac{\rho v^2 d}{\sigma}$	Weber number, expressing the liquid inertia force/the surface tension ratio
$\Pi_4 = C_p$	representing the effect of particle concentration
$\Pi_5 = \frac{d_p}{d}$	representing the effect of particle size

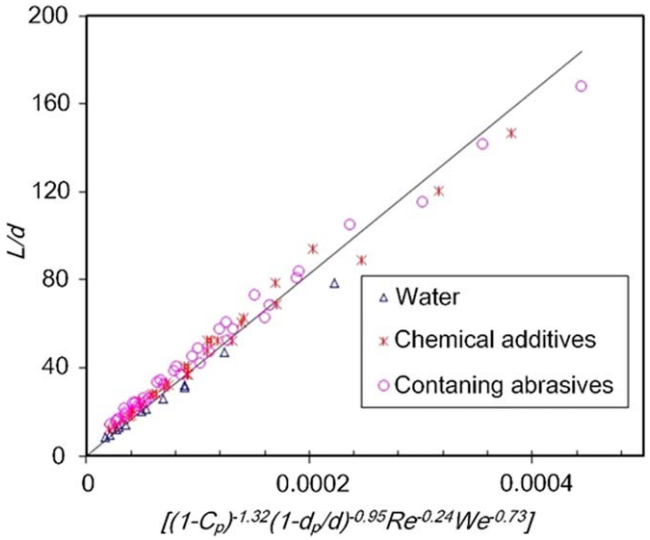

Figure 10. Model predictions (solid line) versus experimental measurements (dots). Reprinted from [36], Copyright (2008), with permission from Elsevier.

The power law formulation approach was applied to further develop equation (1) in which the coefficient and exponents of the power law equation were obtained using multi-variable regression of the experimental data. At a 95% confidence level, it gave

$$\frac{L}{d} = 4.1 \times 10^5 (1 - C_p)^{-1.32} \left(1 - \frac{d_p}{d}\right)^{-0.95} Re^{-0.24} We^{-0.73}, \quad (2)$$

where units of the parameters are in SI system. Figure 10 shows the relationship expressed in equation (2), where experimental data are also plotted for comparison.

It can be concluded that the jet stability can be strengthened by the addition of polymeric additives that increases the liquid viscosity. By contrast, the friction between the surrounding air and the jet surface promotes jet break-up, and this external effect increases when increasing the jet velocity. The parametric model developed provides an essential means towards optimizing the liquid and jetting parameters to maximize the jet stability and ultimately to enhance the cutting performance of microjets.

4.2. Process performance

It is clear that the micromachining technology using a microjet can create a cut or channel with a wider top and narrower bottom, so that a kerf taper is formed, as approximated and shown in figure 11 [44], with the geometry that includes the channel depth (h), the top channel width (w) and the channel wall angle (ϕ). These characteristics of the machined features as well as material removal rate (MRR) are of major concern in practice. Models for estimating these micromachining performance measures for given target material properties have been developed such as those in [44].

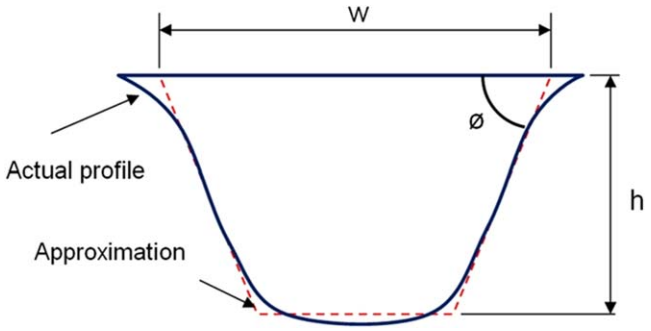

Figure 11. Approximation of the channel cross section. Reprinted from [44], Copyright (2012), with permission from Elsevier.

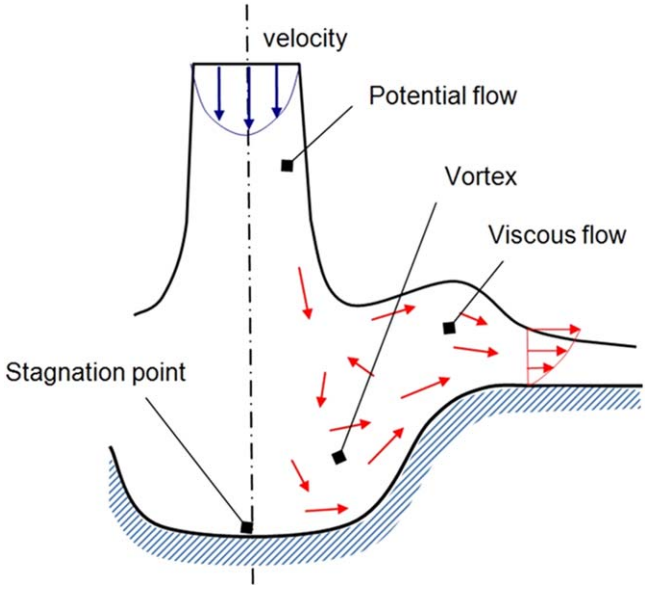

Figure 12. Schematic of the flows developed by the jet impingement in the creation on a channel. Reprinted from [44], Copyright (2012), with permission from Elsevier.

Figure 12 presents a schematic of the flows developed upon the jet impact on a surface. As discussed in [44, 45], the jet kinetic energy that is directly transferred to the abrasive particles plays a major role in forming the depth of channel, while the formation of the channel width is governed by the viscous flow. The expansion of the flow is constrained by the created channel sidewall where vortices are generated. Such vortices form a turbulent flow that drives the particles accumulated at the bottom of the channel and contributes to the formation of channel wall inclination. The features of the channel therefore can be analysed based on the main causes, including the jet kinetic energy, properties of the target material and particle, dynamic properties of the fluid, and dynamics of the nozzle motion. A semi-analytical approach has been used to develop the models [2, 37].

4.2.1. Jet kinetic energy. As the erosion takes place by the motion of abrasive particles, the kinetic energy can be approximated as

$$\frac{dKE}{dt} \approx \frac{1}{2}\dot{m}_p {v_p}^2, \tag{3}$$

where v_p is the average velocity of particles impacting on the material, and $\dot{m}_p$ is the mass flow rate of abrasive particles through the nozzle which is given by

$$\dot{m}_p = C_p \rho_p v_j \frac{\pi d_n^2}{4} \tag{4}$$

in which ρ_p is the density of the particle, d_n is the nozzle diameter and C_p is the percentage particle concentration by mass.

Since the slurry is considered to be uniformly mixed, the particle velocity (v_p) can be assumed to be equal to the slurry velocity (v_j) at the nozzle exit, i.e.

$$v_p \approx v_j. \tag{5}$$

From Bernoulli's principle, the jet velocity can be determined as

$$v_j = k_d \frac{2P}{\rho_s}, \tag{6}$$

where P is the water pressure, ρ_s is the density of the slurry and k_d is a discharge factor to account for velocity loss during jet formation due to nozzle wall friction, and fluid flow disturbances of the slurry.

4.2.2. Properties of the target material and particle. Volume of the target material removed by an abrasive particle (V) is computed using the model proposed by Hutchings [28], i.e.

$$V = C_m {d_p}^3 \frac{\rho_p {d_p}^2}{H_m}, \tag{7}$$

where C_m is the coefficient that accounts for the material property in response to the impact of a particle, including the hardness (H_m), fracture toughness (K_m) and elastic modulus (E_m) of material, i.e.

$$C_m = C_m(H_m, K_m, E_m). \tag{8}$$

4.2.3. Dynamic properties of the fluid. The viscous behaviour of a flow depends on the fluid properties of the slurry, i.e. the dynamic fluid viscosity (μ) and surface tension (σ). The abrasive-water slurry is treated as a non-Newtonian fluid with the dynamic fluid viscosity, μ as shown [46]

$$\mu = K\dot{\gamma}^{n-1}, \tag{9}$$

where $\dot{\gamma}$ is the shear rate, and K and n are the consistency and the flow behaviour indexes of the slurry, respectively. K and n are the constitutive properties which for a given fluid, is a function of the particle contained (C_p) and the size of particles (d_p) in the slurry, i.e.

$$K = K(C_p, d_p), \tag{10}$$

$$n = n(C_p, d_p). \tag{11}$$

For a given controlled volume, the shear rate caused by a given slurry can be considered as a function of the jet velocity at the impact zone [47], i.e.

$$\dot{\gamma} = \dot{\gamma}(v_j). \tag{12}$$

From equations (9)–(12),

$$\mu = \mu(C_p, d_p, v_j). \tag{13}$$

According to the reported studies [48, 49], the increase of particle concentration can lead to an increase in the interfacial surfaces and the absorption of particles in slurry, which in turn results in an increase in the dynamic surface tension of the slurry. Further, the absorption of the particles is limited by the size of the particles contained in the slurry. The dynamic surface tension of slurry therefore can be expressed in the form as

$$\sigma = \sigma(C_p, d_p, v_j). \tag{14}$$

4.2.4. Dynamics of the nozzle motion. The nozzle traverse speed, v_n governs the time that the jet is in contact locally with the target material, thus determining the channel depth. This is particular important in the low pressured microjet machining. As discussed above in section 3.1, the low pressure jet is susceptible to the external influences such as mechanical vibrations from the equipment pressure fluctuation. The major wave formed at the bottom of the channel influences on the MMR.

From the above analysis, the volumetric MRR can be expressed in a general form as

$$MRR = f(d_p, \rho_p, C_p, v_p, v_n, d_n, H_m, E_m, K_m). \tag{15}$$

Following the Buckingham Pi theorem and applying the power law, equation (15) can be expressed in the dimensionless form as

$$\frac{MRR}{{d_p}^2 v_p} = k_1\left(\frac{\rho_p {v_p}^2}{H_m}\right)^{a_1}(C_p)^{b_1}\left(\frac{v_n}{v_p}\right)^{c_1}\left(\frac{d_n}{d_p}\right)^{d_1}\left(\frac{E_m}{H_m}\right)^{e_1}\left(\frac{K_m}{H_m {d_p}^{0.5}}\right)^{f_1} = 0. \tag{16}$$

For convenience, v_p can be represented by the equipment parameter of P, such that

$$MRR = \left(k_2 d_p^2 \frac{\sqrt{P}}{\sqrt{\rho_s}}\right)\left(\frac{\rho_p P}{H_m \rho_s}\right)^{a_2}(C_p)^{b_2}\left(\frac{v_n\sqrt{\rho_s}}{\sqrt{P}}\right)^{c_2}\left(\frac{d_n}{d_p}\right)^{d_2}\left(\frac{E_m}{H_m}\right)^{e_2}\left(\frac{K_m}{H_m {d_p}^{0.5}}\right)^{f_2}. \tag{17}$$

Similarly, the channel angle, ϕ, can be expressed as

$$\varnothing = k_4\left(\frac{\rho_p P}{H_m \rho_s}\right)^{a_4}(C_p)^{b_4}\left(\frac{v_n\sqrt{\rho_s}}{\sqrt{P}}\right)^{c_4}\left(\frac{d_n}{d_p}\right)^{d_4}\left(\frac{E_m}{H_m}\right)^{e_4}\left(\frac{K_m}{H_m {d_p}^{0.5}}\right)^{f_4}. \tag{18}$$

To determine the constants in equations (17) and (18), an experimental work has been conducted. The test specimens used were 5 mm thick amorphous soda-lime glass sheets, the same material as that used in the hole drilling study of this paper. Alumina abrasives with the average diameter $d_p = 25\,\mu$m were used. Table 2 shows the operating parameters for machining micro-channels.

Table 2. Operating parameters for micro-channel machining. Reprinted from [44], Copyright (2012), with permission from Elsevier.

Water pressure, P (MPa)	8, 10, 12 and 14
Nozzle traverse speed, v_n (mm s^{-1})	0.15, 0.20, 0.25 and 0.30
Particle concentration, C_p (% by mass)	15, 20, 25 and 30
Nozzle standoff distance, S_n (mm)	3, 4, 5, 6

By regression analysis of the experimental data at 95% confidence level, equations (17) and (18) become

$$MRR = (1.99 \times 10^{-22})\left(\frac{P}{\rho_s}\right)^{1.83}(C_p)^{1.78}\left(\frac{v_n\sqrt{\rho_s}}{\sqrt{P}}\right)^{-0.78}, \tag{19}$$

$$\phi = (771 \times 10^{-10})\left(\frac{P}{\rho_s}\right)^{0.34}(C_p)^{1.27}\left(\frac{v_n\sqrt{\rho_s}}{\sqrt{P}}\right)^{-0.1.45}, \tag{20}$$

where units are in SI system.

From the approximation of the channel cross section shown in figure 11, the channel depth can be determined, i.e.

$$h = \frac{w + \sqrt{w^2 - (4MRR/v_n)\cos\phi}}{2\cos\phi}. \tag{21}$$

The top channel width can be determined from a regression analysis of experimental data where a backward elimination procedure was employed to eliminate those variables that have only minor or negligible effect on the channel width. The regression model is given by

$$w = 2.34 \times 10^{-18}P^2 - 2.5 \times 10^{-11}P + 4.79 \times 10^4. \tag{22}$$

A quantitative assessment of the models was made, based on the percentage deviation of the model predictions with respect to the experimental results under the corresponding conditions [41]. It can be concluded that the models can provide an adequate predication for the channel feature dimensions and MRR under the test conditions considered.

It is noted that due to the lower kinetic energy possessed by the jet, the factors that affect the formation of micro-channels are very much different from those of the ultrahigh pressure AWJ meso-machining process. This is notably attributed to the secondary material removal process induced by the viscous flow that causes the particles to impact the material surface at a shallower angle. The shallower impact angle results in a ductile-mode-like erosion even on a brittle material.

5. Vibration assisted microjet machining

There have been numerous reported works where ultrasonic vibration assistance is employed to improve the machining process. Vibration has also been used to assist microjet machining process [50, 51] although the mechanisms beyond which the vibration affects the machining process and

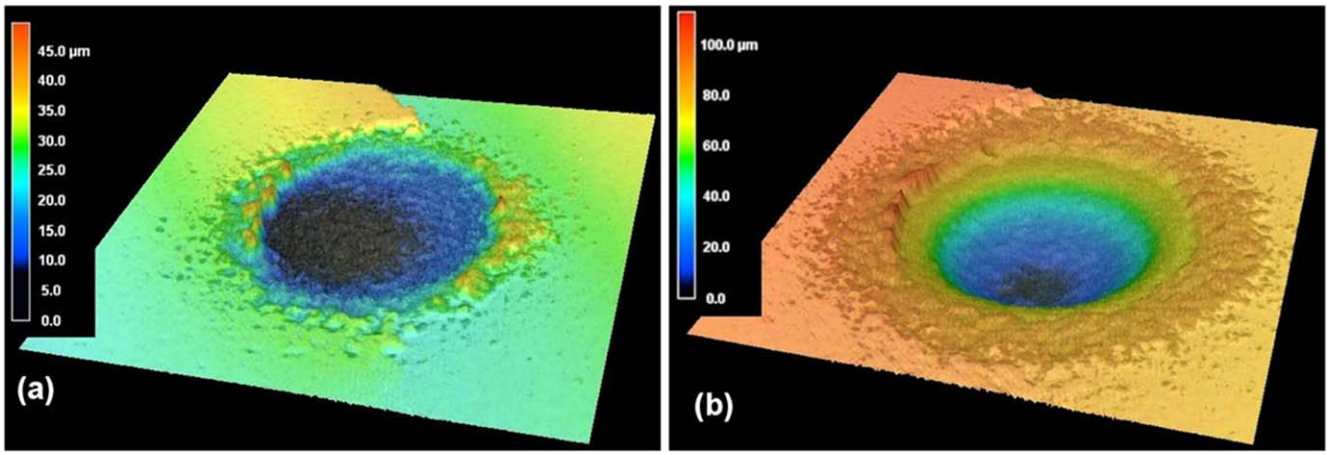

Figure 13. Hole features obtained on SiC surface after 30 s of processing by a 120 m s^{-1} slurry jet of 125 μm in diameter containing 25 μm SiC abrasives at 15% concentration: (a) without vibration and (b) with vibration.

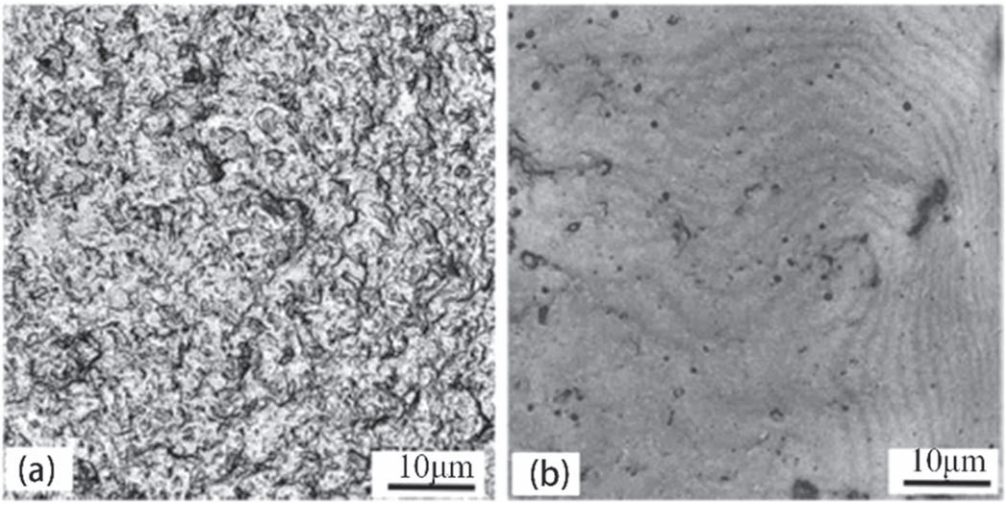

Figure 14. Surface topology of SiC after 30 s of processing by a slurry jet described in figure 13: (a) without vibration and (b) with vibration.

performance may be different from those in traditional machining where solid tools are used [52, 53]. In a recent study at the authors' laboratory, ultrasonic vibration of 20 kHz was applied perpendicularly on the target material surface with the amplitude in an order of ten micrometres. The target material was single crystal 4H-SiC thin film of 350 μm in thickness. This type of material is considered to be extremely hard and brittle, ranked as third in the hardness scale after diamond and cubic boron nitride (CBN) [1]. The work used a 125 μm diameter nozzle and SiC abrasives with the concentration varying up to 15%. The jet velocity was characterised as fully turbulent with the velocity above 120 m s^{-1}.

Figure 13 shows the typical hole features obtained from microjet machining without and with vibration assistance. It was found that vibration assistance could enhance the MRR. The hole processed with the vibration assistance had the depth of 18 times greater than that obtained with the same machining condition but without the assistance of vibration. It was interesting to find that not only the MRR, but also the surface finish that was significantly improved, as shown in figure 14. It is noticed that in spite of the material's brittleness and the tendency of brittle failure, ductile deformation was found to be dominant on the SiC surface processed with vibration assisted microjet. Details of this finding will be reported separately.

6. Conclusions

A micro scale of the ultrahigh pressure AWJ is capable of machining micro part geometrical features. While it earns the various advantages of AWJ, it can provide a ductile-like material removal on the processed surface regardless of the material's brittleness. The characteristics of the machined surface and features are a result of different wear processes associated with the change of flow regimes developed on the surface. The viscous flow generated upon the jet impact induces a shearing action which is a key mechanism that promotes the ductile-like removal mode. Relevant models have been developed for estimating the jet and process performance. With the assistance of

vibration, it is feasible to extend the technology to processing extremely hard and brittle materials, in which the vibration does not only enhance the MRR, but also the surface finish. Further work is being undertaken to optimise the operating parameters for a balance between the productivity and the high demand for machined surface integrity.

References

[1] Saurav G 2014 The current understanding on the diamond machining of silicon carbide *J. Phys. D: Appl. Phys.* **47** 243001

[2] Chen Y, Nguyen T and Zhang L C 2009 Polishing of polycrystalline diamond by the technique of dynamic friction—Part 5: quantitative analysis of material removal *Int. J. Mach. Tools Manuf.* **49** 515–20

[3] Patten J, Gao W and Yasuto K 2004 Ductile regime nanomachining of single-crystal silicon carbide *J. Manuf. Sci. Eng.* **127** 522–32

[4] Shinji M, Sin'ya M, Toshiya Y, Hiroaki A and Susumu N 1981 Reactive ion-beam etching of silicon carbide *Japan. J. Appl. Phys.* **20** L38

[5] Zhao Y, Kunieda M and Abe K 2016 Challenge to EDM slicing of single crystal SiC with blade electrode utilizing a reciprocating worktable *Procedia CIRP* **42** 185–90

[6] Borowiec A and Haugen H K 2004 Femtosecond laser micromachining of grooves in indium phosphide *Appl. Phys.* A **79** 521

[7] Nguyen T, Zarudi I and Zhang L C 2007 Grinding-hardening with liquid nitrogen: mechanisms and technology *Int. J. Mach. Tools Manuf.* **47** 97–106

[8] Ke K, Joglekar A P, Hsiao-hua L, Meyhofer E, Hasselbrink E, Mourou G and Hunt A J 2005 The physics and limits of femtosecond laser micromachining *(CLEO) Conf. on Lasers and Electro-Optics*

[9] Wang J 2003 *Abrasive Waterjet Machining of Engineering Materials* (Zurich: Trans Tech)

[10] Summers D 1984 *Waterjetting Technology.* (London: Chapman and Hall)

[11] Nguyen T, Liu D, Thongkaew K, Li H, Qi H and Wang J 2018 The wear mechanisms of reaction bonded silicon carbide under abrasive polishing and slurry jet impact conditions *Wear* **410–411** 156–64

[12] Liu H T 2010 Waterjet technology for machining fine features pertaining to micromachining *J. Manuf. Process.* **12** 8–18

[13] Nouraei H, Wodoslawsky A, Papini M and Spelt J K 2013 Characteristics of abrasive slurry jet micro-machining: a comparison with abrasive air jet micro-machining *J. Mater. Process. Technol.* **213** 1711–24

[14] McCarthy M J and Molloy N A 1974 Review of stability of liquid jets and the influence of nozzle design *Chem. Eng. J.* **7** 7–20

[15] Humphrey J A C 1990 Fundamentals of fluid motion in erosion by solid particle impact *Int. J. Heat Fluid Flow* **11** 170–95

[16] Momber A W and Kovacevic R 1998 *Principles of Abrasive Water Jet Machining* (Berlin: Springer)

[17] Nguyen T, Pang K and Wang J 2009 A preliminary study of the erosion process in micro-machining of glasses with a low pressure slurry jet *Key Eng. Mater.* **389–90** 375–80

[18] Wang J, Nguyen T and Pang K 2009 Mechanisms of microhole formation on glasses by an abrasive slurry jet *J. Appl. Phys.* **105** 044906

[19] Pang K L 2011 A study of the abrasive waterjet micro-machining for amorphous glasses *PhD Thesis* School of Mechanical and Manufacturing Engineering, The University of New South Wales

[20] McLean R H 1964 Crossflow and impact under jet bits *J. Petrolium Technol.* **16** 1299–306

[21] Yanaida K 1974 Flow characteristics of waterjet *2nd Int. Symp. on Jet Cutting Technology BHRA Fluid Engineering (Cranfield, Bedford)*

[22] Bhunia S K and Lienhard V J H 1994 Surface disturbance evolution and the splattering of turbulent liquid jets *J. Fluids Eng.* **116** 721–7

[23] Wensink H and Elwenspoek M C 2002 A closer look at the ductile–brittle transition in solid particle erosion *Wear* **253** 1035–43

[24] Wang J and Li W Y 2016 A new look into the loose particle impact process for ductile materials *Mater. Sci. Forum* **874** 213–8

[25] Zeng J and Kim T J 1996 An erosion model for abrasive waterjet milling of polycrystalline ceramics *Wear* **199** 275–82

[26] Bitter J G A 1963 A study of erosion phenomena: Part II *Wear* **6** 169–90

[27] Gerhart P M 1992 *Fundamentals of Fluid Mechanics* (Harlow: Addison-Wesley)

[28] Hutchings I M 1992 *Tribology: Friction and Wear of Engineering Materials* (London: Edward Arnold)

[29] Paik U, Park H C, Choi S C, Ha C G, Kim J W and Jung Y G 2002 Effect of particle dispersion on microstructure and strength of reaction-bonded silicon carbide *Mater. Sci. Eng.* **334** 267–74

[30] Toulemont Y, Breysse J, Piepot D and Miura S 2004 The 3.5-m all-SiC telescope for SPICA *Proc. SPIE* **5487** 1001–12

[31] Yoshida M, Onodera A, Ueno M, Takemura K and Shimomura O 1993 Pressure-induced phase transition in SiC *Phys. Rev.* B **48** 10587–90

[32] Agarwal S and Rao P V 2008 Experimental investigation of surface/subsurface damage formation and material removal mechanisms in SiC grinding *Int. J. Mach. Tools Manuf.* **48** 698–710

[33] Zarudi I, Nguyen T and Zhang L C 2005 Effect of temperature and stress on plastic deformation in monocrystalline silicon induced by scratching *Appl. Phys. Lett.* **86** 011922

[34] Jang J, Lance M J, Wen S, Tsui T Y and Pharr G M 2005 Indentation-induced phase transformations in silicon: influences of load, rate and indenter angle on the transformation behavior *Acta Mater.* **53** 1759–70

[35] Budnitzki M and Kuna M 2016 Stress induced phase transitions in silicon *J. Mech. Phys. Solids* **95** 64–91

[36] Nguyen T, Shanmugam D K and Wang J 2008 Effect of liquid properties on the stability of an abrasive waterjet *Int. J. Mach. Tools Manuf.* **48** 1138–47

[37] Nguyen T and Zhang L C 2005 Modelling of the mist formation in a segmented grinding wheel system *Int. J. Mach. Tools Manuf.* **45** 21–8

[38] Lefebvre A H 1989 *Atomization and Spray* (Washington DC: Taylor and Francis)

[39] Grant R P and Middleman S 1966 Newtonian jet stability *AIChE J.* **12** 669–78

[40] Kitamura Y and Takahashi T 1976 Stability of a liquid jet in air flow normal to the jet axis *J. Chem. Eng. Japan* **9** 282–6

[41] Dombrowski N and Johns W R 1963 The aerodynamic instability and disintegration of viscous liquid sheets *Chem. Eng. Sci.* **18** 203–14

[42] Zhang J and Pelton R 1999 The surface tension of aqueous poly(N-isopropylacrylamide-co-acrylamide) *J. Polym. Sci.* A **37** 2137–43

[43] Bayvel L and Orzechowski Z 1993 Liquid atomization *Combustion (An International Series)* (London: Taylor and Francis)

[44] Pang K, Nguyen T, Fan J M and Wang J 2012 Modelling of the micro-channelling process on glasses using an abrasive slurry jet *Int. J. Mach. Tools Manuf.* **53** 118–26
[45] Pang K, Nguyen T, Fan J and Wang J 2012 A study of micro-channeling on glasses using an abrasive slurry jet *Mach. Sci. Technol.* **16** 547–63
[46] Tanner R 2000 *Engineering Rheology* 2nd ed. (NewYork: Oxford University Press)
[47] Valko P and Economides M 1995 *Hydraulic Fracture Mechanics.* (Chichester, England: Wiley)
[48] Brian B W and Chen J C 1987 Surface tension of solid–liquid slurries *AIChE J.* **33** 316–8
[49] Kihm K D and Deignan P 1995 Dynamic surface tension of coal-water slurry fuels *Fuel* **74** 295–300
[50] Zhu H T, Huang C Z, Wang J, Liu Z W and Zhang S G 2010 Erosion mechanism of ultrasonic vibration abrasive waterjet in micro machining *Key Eng. Mater.* **443** 675–80
[51] Zhang Z W, Zhu H T, Huang C Z, Wang J, Yao P and Liu Z W 2013 A study on erosion performance of monocrystalline silicon in ultrasonic vibration-assisted abrasive water jet machining *Adv. Mater. Res.* **797** 39–45
[52] Zhou M, Wang X J, Ngoi B K A and Gan J G K 2002 Brittle–ductile transition in the diamond cutting of glasses with the aid of ultrasonic vibration *J. Mater. Process. Technol.* **121** 243–51
[53] Huda A H N F, Ascroft H and Barnes S 2016 Machinability study of ultrasonic assisted machining (UAM) of carbon fibre reinforced plastic (CFRP) with multifaceted tool *Procedia CIRP* **46** 488–91